Spatially-localized wavelet-based spectral analysis of preferential concentration in particle-laden turbulence

By M. Bassenne, J. Urzay AND P. Moin

1. Motivation and objectives

In this study, the wavelet transform is used to address the preferential concentration of inertial particles in one-way coupled, particle-laden incompressible homogeneous-isotropic turbulence. The analysis includes a characterization of the spatially-localized spectral structure of turbulence in the vicinity of the particle clouds, along with a spectral analysis of the particle concentration field. The spatial localization of spectral quantities is enabled here by the utilization of wavelets instead of Fourier transforms.

2. Background

Preferential concentration of particles is an ubiquitous phenomenon in multi-phase turbulent flows (Balachandar & Eaton 2010). The wide range of scales and different topological flow structures present in high-Reynolds number flows cause accumulation of particles in distinct regions whose properties are difficult to characterize. The spatial inhomogeneities arising in the concentration of particles as a result of the preferential-concentration effect have important consequences on the relative dispersion and inter-phase coupling with the turbulent environment.

Theoretical studies of preferential concentration of particles are limited given the complex coupling of particle motion with the unsteady and multi-scale turbulence dynamics. However, they have drawn a number of fundamental conclusions, some of which are connected to the present study. In particular, Robinson (1956) was the first to establish an analytical framework for the accumulation of particles by noticing that the disperse phase is compressible, and that in irrotational incompressible flows the particle number density n increases monotonically in the Lagrangian frame according to the corresponding mass conservation equation for particles

$$\frac{1}{n}\frac{\mathrm{D}n}{\mathrm{D}t} = -\frac{\partial u_{p,i}}{\partial x_i} > 0, \tag{2.1}$$

where D is the material derivative, t is the time and $u_{p,i}$ is the particle velocity. In particular, an expression for the right hand side of Eq. (2.1) can be obtained by taking the divergence of the Eulerian version of the equation of motion for the particles

$$\frac{4}{3}\pi\rho_p a^3\frac{\mathrm{D}u_{p,i}}{\mathrm{D}t} = 6\pi\rho\nu a(u_i - u_{p,i}), \tag{2.2}$$

which leads to

$$t_a\frac{\mathrm{D}}{\mathrm{D}t}\left(\frac{\partial u_{p,i}}{\partial x_i}\right) + \frac{\partial u_{p,i}}{\partial x_i} = 2Q_p t_a, \tag{2.3}$$

where

$$t_a = \frac{2}{9}\frac{\rho_p}{\rho}\frac{a^2}{\nu} \tag{2.4}$$

is the characteristic particle acceleration time, and

$$Q_p = -\frac{1}{2}\frac{\partial u_{p,i}}{\partial x_j}\frac{\partial u_{p,j}}{\partial x_i} = \frac{1}{4}\left(\omega_{p,k}\omega_{p,k} - 2S_{p,ij}S_{p,ij}\right) \tag{2.5}$$

is the second invariant of the particle velocity-gradient tensor. In this formulation, $S_{p,ij} = (1/2)\left(\partial u_{p,i}/\partial x_j + \partial u_{p,j}/\partial x_i\right)$ is the strain rate of the particle velocity field, and $\omega_{p,i} = \varepsilon_{ijk}\partial u_{p,k}/\partial x_j$ the associated vorticity, with ε_{ijk} the permutation tensor. Additionally, a is the particle radius, ρ_p the particle density, and ν and ρ are the carrier-phase kinematic viscosity and density, respectively. Small particle Reynolds numbers, along with large density ratios $\rho_p/\rho \gg 1$, have been assumed in writing Eq. (2.3).

Since $Q_p < 0$ in irrotational flows, integration of (2.3), subjected to the initial condition $\partial u_{p,i}/\partial x_i = 0$ at $t = 0$, gives $\partial u_{p,i}/\partial x_i = 2\exp(-t/t_a)\int_0^t Q_p \exp(t/t_a)dt < 0$, which corresponds to an accumulation of particles along streamlines that is described by substituting this expression into Eq. (2.1). Conversely, the presence of vorticity in the carrier phase, $\omega_i = \varepsilon_{ijk}\partial u_k/\partial x_j$, induces vorticity in the disperse phase, as easily observed by taking the curl of Eq. (2.2), which gives

$$\frac{\mathrm{D}\omega_{p,i}}{\mathrm{D}t} + \omega_{p,i}\frac{\partial u_{p,k}}{\partial x_k} - \omega_{p,j}\frac{\partial u_{p,i}}{\partial x_j} = \frac{\omega_i - \omega_{p,i}}{t_a}, \tag{2.6}$$

where ω_i appears as a source term. The resulting vorticity in the disperse phase leads to sign variations in Q_p, by which dispersion originates from predominantly vortical regions. Subsequent studies on aerodynamic focusing of particles have largely exploited these fundamental results (Fernández De La Mora & Riesco-Chueca 1988). Similarly, Robinson's inequality (2.1) has implications on the dynamics of fuel sprays in counterflow mixing layers (Sánchez *et al.* 2015), where small droplets tend to accumulate near the stagnation plane by the action of the strain rate unless the temperature of one of the streams is sufficiently high to enable vaporization.

In a related study, Maxey (1987) recognized that (2.3) simplifies to

$$\frac{\partial u_{p,i}}{\partial x_i} = 2Qt_a \tag{2.7}$$

for particle acceleration times t_a much smaller than the characteristic fluid mechanical time $|Q|^{-1/2}$, where

$$Q = -\frac{1}{2}\frac{\partial u_i}{\partial x_j}\frac{\partial u_j}{\partial x_i} = \frac{1}{4}\left(\omega_k\omega_k - 2S_{ij}S_{ij}\right) \tag{2.8}$$

is the second invariant of the carrier-phase velocity-gradient tensor, with the norm of the strain-rate tensor $S_{ij} = (1/2)\left(\partial u_i/\partial x_j + \partial u_j/\partial x_i\right)$ competing against the enstrophy in modulating particle accumulation. As a result, particles are predicted to accumulate in regions of high strain rate and low vorticity. It should be emphasized, however, that Eq. (2.7) is an asymptotic approximation for small particle inertia, with finite inertial effects entering into the problem to decorrelate the dynamics of the carrier phase, Q, from those of the disperse phase, Q_p.

In spite of the limitations described above, the physical arguments implied by Eq. (2.7) are useful and easily observed in numerical simulations and experiments. For instance, the computational results presented in Figure 1(a), obtained from DNS of one-way coupled

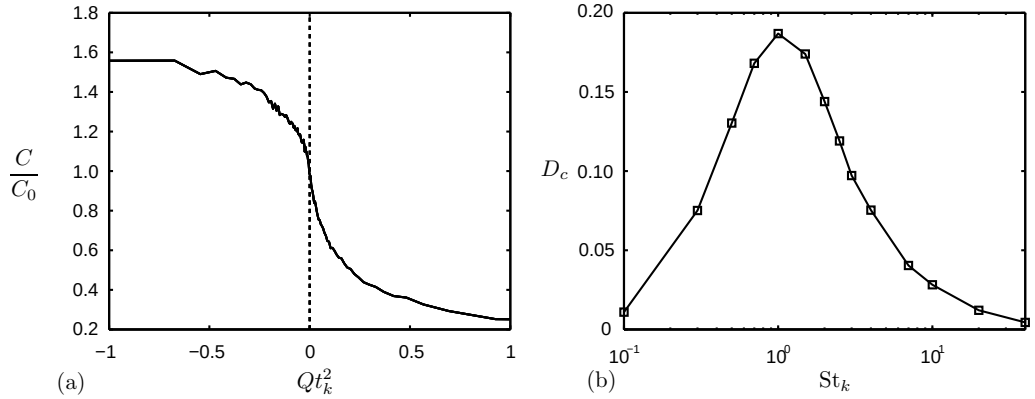

FIGURE 1. (a) Conditional expectation of the particle concentration C normalized by its mean C_0 as a function of the second invariant of the velocity-gradient tensor for $\mathrm{St}_k = 1$, and (b) preferential-concentration global indicator D_c as a function of the Stokes number.

homogeneous-isotropic particle-laden turbulence (see Section 4 for further details) show that the conditional expectation of the particle concentration C is strongly negatively correlated with Q, confirming that particles are predominantly found outside swirling regions (where $Q > 0$) and tend to accumulate in highly-strained zones (where $Q < 0$).

A complementary representation of preferential concentration in homogeneous-isotropic turbulence can be obtained by examining the dependence of the accumulation factor

$$D_c = \sum_{C=0}^{N_p} \left[p_c(C) - P_c(C)\right]^2 \tag{2.9}$$

on the Stokes number

$$\mathrm{St}_k = t_a/t_k, \tag{2.10}$$

where $p_c(C)$ is the fraction of computational cells containing C particles, $P_c(C)$ is the discrete Poisson probability density function (PDF), N_p is the number of particles, and $t_k = (\nu/\epsilon)^{1/2}$ is the Kolmogorov time scale, with ϵ the turbulent dissipation. In particular, positive deviations from $D_c = 0$ represent departures from a random distribution of particle concentration. Values $D_c > 0$ are therefore ascribed to preferential concentration of particles (Squires & Eaton 1991), which becomes maximum at Stokes numbers $\mathrm{St}_k \sim 1$ in homogeneous-isotropic turbulence, as shown in Figure 1(b).

Computational analyses of preferential concentration in particle-laden turbulence are typically performed in physical and spectral spaces, the latter addressed always using Fourier transforms (Squires & Eaton 1991; Wang & Maxey 1993; Ferrante & Elghobashi 2003; Jin *et al.* 2010). In particular, analyses of results in physical space, such as the ones presented in Figure 1, provide global statistics of the turbulence preferentially sampled by particles, and therefore do not provide any scale dependency. For instance, although Figure 1(a) shows that particles are found away from swirling regions, it does not provide any insight into the scales associated with those zones. Since particles are never found in highly vortical regions and vorticity lives in the small scales of turbulence, based on Figure 1(a) it may be erroneously concluded that the characteristic particle concentration variations occur over much broader regions whose sizes are associated with those bearing low vorticity, such as the integral scales of turbulence.

To circumvent the limitations of investigations in physical space, Fourier-based spectral

analyses can be used to obtain scale-dependent information. However, the scale dependency provided by the spectral localization properties of the Fourier transform is counterbalanced with the associated spatial delocalization with regard to where in space those dependencies are found. In this way, the accurate spectral insight gained with Fourier transforms pertains to spatially-averaged dynamics. In contrast, spatial localization in spectral space can be obtained by using wavelets. In particular, wavelets are spatially localized wave-like oscillations that serve as basis functions for the spectral decomposition of scalar and velocity fields. The capability of wavelets for drawing information simultaneously in both space and wavenumber domains is a distinct characteristic that cannot be achieved with traditional Fourier transforms. In recent years, wavelets have been applied to the analysis of a multitude of diverse physical phenomena, including turbulent flows, where they demonstrated potential to identify and characterize localized flow structures in a way that brings new insights into turbulence analysis, modeling and simulation (Farge & Rabreau 1988; Meneveau 1991; Schneider & Vasilyev 2010).

In this study, the preferential concentration of particles in one-way coupled, incompressible homogeneous-isotropic turbulence is computationally studied in spectral space using wavelets, which render localized scale-dependent statistical information regarding the turbulence structures associated with variations in the spatial distribution of particles. This report is organized as follows. A brief summary of the formulae involved in the wavelet spectral representation is provided in Section 3. The computational setup is described in Section 4. Numerical results, including scale-dependent spatially localized statistics of preferential concentration, are given in Section 5. Lastly, conclusions are drawn in Section 6.

3. Wavelet spectral representation of particle-laden turbulence

In this section, a brief description of the discrete wavelet transform, including corresponding spectral statistics, is provided. The reader is referred to other papers for more detailed explanations of the method (Mallat 1989; Meneveau 1991). For illustration, consider a three dimensional discrete turbulent scalar field φ, described in physical space by its point-wise values $\varphi(\boldsymbol{x})$, where $\boldsymbol{x} = (i\Delta, j\Delta, k\Delta)$ denotes collocation points, with i, j and $k = 0, 1, \dots N-1$. In this formulation, Δ is the grid spacing, $N = L/\Delta + 1$ the number of grid points in each direction, and L the computational domain side length. This representation assumes a uniform discretization of a cubic computational domain in accordance with the numerical setup described in Section 4.

If φ is triply-periodic, it is also uniquely described by the discrete Fourier transform

$$\widehat{\varphi}(\boldsymbol{\kappa}) = \langle \varphi(\boldsymbol{x}) f^{\boldsymbol{\kappa}}(\boldsymbol{x}) \rangle_{\boldsymbol{x}} \,, \tag{3.1}$$

where $\boldsymbol{\kappa} = (2\pi i/L, 2\pi j/L, 2\pi k/L)$ is a wavenumber vector, $f^{\boldsymbol{\kappa}}$ are orthonormal Fourier-basis functions, and the bracketed operator $\langle\cdot\rangle_{\boldsymbol{x}}$ indicates volume averaging by integration with respect to $\boldsymbol{x}$ over the entire computational domain. Parseval's theorem,

$$\big\langle |\varphi(\boldsymbol{x})|^2 \big\rangle_{\boldsymbol{x}} = \sum_{\boldsymbol{\kappa}} |\widehat{\varphi}(\boldsymbol{\kappa})|^2, \tag{3.2}$$

relates the physical-space and Fourier-space representations of the energetics of the scalar φ. It is worth noting that the Fourier transform (3.10) is spectrally localized, yet the resulting information is spatially delocalized. This limitation can be circumvented by the utilization of wavelets, as briefly explained below.

Consider the wavelet transform of φ,

$$\breve{\varphi}(s,\boldsymbol{x_s},d)=\left\langle\varphi(\boldsymbol{x})\psi^{s,\boldsymbol{x_s},d}(\boldsymbol{x})\right\rangle_{\boldsymbol{x}}, \tag{3.3}$$

which quantifies the fluctuations of φ at scale s and position $\boldsymbol{x_s}$. Specifically, $s=(1,\ldots,S)$ are scale exponents, with $S=\log_2 N$ the number of resolution levels (Mallat 1989). Additionally, $\boldsymbol{x_s}=2^s(i\Delta,j\Delta,k\Delta)$ are subsets of collocation points where the wavelets are centered, with $i,j,k=0,1\ldots,N/2^s-1$. The rest of the notation in (3.3) involves the wavelet-directionality index $d=(1,\ldots,7)$ and the set of orthonormal wavelet functions $\psi^{s,\boldsymbol{x_s},d}$. In particular, $\psi^{s,\boldsymbol{x_s},d}$ are taken to be Haar wavelet functions, which are compactly-supported, localized wave-like oscillations characterized by a wavenumber modulus κ given by

$$\kappa=\frac{\pi}{\Delta}\,2^{1-s}, \tag{3.4}$$

or equivalently, by a lengthscale ℓ_s given by

$$\ell_s=2\pi/\kappa=2^s\Delta. \tag{3.5}$$

Similarly to Eq. (3.2), the wavelet components of φ obey

$$\left\langle|\varphi(\boldsymbol{x})|^2\right\rangle_{\boldsymbol{x}}=\sum_{s=1}^{S}\left\langle\sum_{d=1}^{7}|\breve{\varphi}(s,\boldsymbol{x_s},d)|^2\right\rangle_{\boldsymbol{x_s}}, \tag{3.6}$$

indicating that the quantity within the bracketed operator is a local measure of the intensity associated with fluctuations of φ at a length scale ℓ_s in a spatial region centered at $\boldsymbol{x_s}$. In this study, the wavelet-directionality index d is not exploited since the flow is isotropic.

3.1. *Wavelet spectra*

The mean or spatially-averaged wavelet spectrum of φ at scale s is defined as

$$E_\varphi(\kappa)=\frac{2^{-3s}}{\kappa\ln 2}\left\langle\sum_{d=1}^{7}|\breve{\varphi}(s,\boldsymbol{x_s},d)|^2\right\rangle_{\boldsymbol{x_s}}, \tag{3.7}$$

which is analogous to the Fourier spectrum. Conversely, the local spectrum

$$E_\varphi(\kappa,\boldsymbol{x_s})=\frac{2^{-3s}}{\kappa\ln 2}\sum_{d=1}^{7}|\breve{\varphi}(s,\boldsymbol{x_s},d)|^2, \tag{3.8}$$

quantifies the spectral intensity of the fluctuations of φ at location $\boldsymbol{x_s}$, with (3.7) and (3.8) being related as $E_\varphi(\kappa)=\langle E_\varphi(\kappa,\boldsymbol{x_s})\rangle_{\boldsymbol{x_s}}$. Correspondingly, the standard deviation

$$\sigma(\kappa)=\sqrt{\langle E_\varphi(\kappa,\boldsymbol{x_s})^2\rangle_{\boldsymbol{x_s}}-\langle E_\varphi(\kappa,\boldsymbol{x_s})\rangle^2_{\boldsymbol{x_s}}}, \tag{3.9}$$

flatness factor

$$F(\kappa)=\frac{\left\langle E_\varphi(\kappa,\boldsymbol{x_s})^4\right\rangle_{\boldsymbol{x_s}}}{\langle E_\varphi(\kappa,\boldsymbol{x_s})^2\rangle^2_{\boldsymbol{x_s}}}, \tag{3.10}$$

and extrema

$$E^{>}_\varphi(\kappa)=\min_{\boldsymbol{x_s}}E_\varphi(\kappa,\boldsymbol{x_s}),\quad E^{<}_\varphi(\kappa)=\max_{\boldsymbol{x_s}}E_\varphi(\kappa,\boldsymbol{x_s}), \tag{3.11}$$

represent statistical quantities that measure the spatial variabilities of the spectrum.

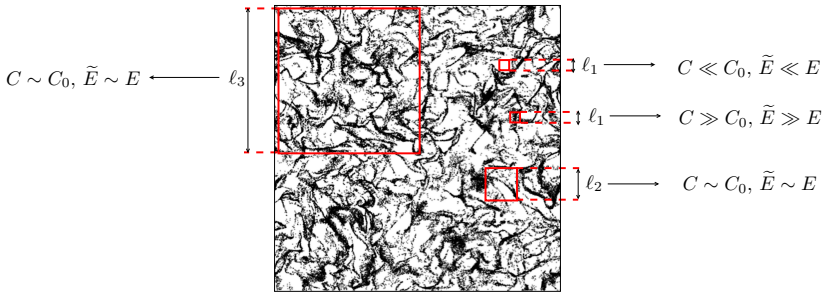

FIGURE 2. Schematics of wavelet multi-resolution effects on concentration-weighted spectra. The figure shows the spatial distribution of particles (black dots) in a 2D cross section of a DNS of particle-laden homogeneous-isotropic turbulence at St_k=1 (see Section 4 for further details).

3.2. *Concentration-weighted spectra*

In this study, the spatially-localized spectral information provided by the wavelet transform (3.3) is exploited to characterize the turbulence sampled preferentially by particles. For this purpose, the local spectrum (3.8) is weighted by the local concentration of particles as

$$\widetilde{E}_\varphi(\kappa) = \frac{\langle C_s(\boldsymbol{x_s}) E_\varphi(\kappa, \boldsymbol{x_s})\rangle_{\boldsymbol{x_s}}}{\langle C_s(\boldsymbol{x_s})\rangle_{\boldsymbol{x_s}}}. \tag{3.12}$$

In Eq. (3.12), the symbol $C_s(\boldsymbol{x_s})$ refers to the Eulerian particle concentration field computed by counting the number of particles in a cubic volume of side length ℓ_s centered at $\boldsymbol{x_s}$, consistently with the scale and spatial location associated with the spectrum $E(\kappa, \boldsymbol{x_s})$. In particular, the spatial average of $C_s(\boldsymbol{x_s})$ corresponds to the mean concentration C_0,

$$\langle C_s(\boldsymbol{x_s})\rangle_{\boldsymbol{x_s}} = C_0. \tag{3.13}$$

For uniformly distributed particles, the concentration-weighted spectrum (3.12) becomes equal to the unweighted spectrum (3.7) at all wavenumbers, $\widetilde{E}_\varphi(\kappa) = E_\varphi(\kappa)$. Note, however, that a spatial distribution of particles segregated in clouds whose characteristic length is in the high-wavenumber range, would render approximately neutral weighting at small wavenumbers, while departures from the unweighted spectra would only be noticed at large wavenumbers. As a result, in homogeneous-isotropic turbulence, weighted and unweighted spectra are approximately equal only in the small wavenumber range where preferential concentration is not discernible. These considerations are illustrated schematically in Figure 2.

4. Computational setup

In this study, a DNS of incompressible homogeneous isotropic turbulence laden with point particles is performed in a triply-periodic domain. The mass-loading ratio is sufficiently small such that the influences of the particles on the gas are negligible. The numerical integrations involve the linearly-forced Navier-Stokes equations

$$\frac{\partial u_i}{\partial x_i} = 0, \tag{4.1}$$

$$\frac{\partial u_i}{\partial t} + u_j \frac{\partial u_i}{\partial x_j} = -\frac{1}{\rho}\frac{\partial p}{\partial x_i} + \nu \frac{\partial^2 u_i}{\partial x_j \partial x_j} + A u_i, \tag{4.2}$$

where p is the hydrodynamic pressure. The forcing coefficient A is given by

$$A(t) = \frac{\epsilon(t) - G[k(t) - k_\infty]/t_\ell}{2k(t)}, \tag{4.3}$$

which yields statistically steady homogeneous-isotropic turbulence at constant kinetic energy (Bassenne *et al.* 2015). In this formulation, $k(t) = \langle u_i u_i \rangle_{\boldsymbol{x}}/2$ is the instantaneous turbulent kinetic energy, k_∞ is the steady value of the turbulent kinetic energy, $\epsilon(t) = \langle \nu(\partial u_i/\partial x_j)(\partial u_i/\partial x_j)\rangle_{\boldsymbol{x}}$ is the instantaneous turbulent dissipation, $t_\ell = (2k_\infty/3\epsilon_\infty)^{1/2}$ is the integral time, with ϵ_∞ the steady value of the turbulent dissipation, and $G \gg 1$ is a dimensionless constant that defines a short characteristic control time $t_\ell/G \ll t_a$ during which the kinetic energy converges to k_∞ at the beginning of the simulations.

The initial conditions used for integrating (4.1)-(4.2) involve a synthetic, solenoidal-isotropic velocity field with a prescribed energy spectrum that serves as a starting point for the computations. Such a field is generated by employing the Passot-Pouquet kinetic-energy model spectrum (Passot & Pouquet 1987) and by subsequently calculating the corresponding initial velocity components u_i from their Fourier transforms subject to random phases and a divergence-free condition.

The formulation of the disperse phase is based on a Lagrangian description for small particles that satisfy $a/\ell_k \ll 1$, with $\ell_k = (\nu^3/\epsilon_\infty)^{1/4}$ the Kolmogorov length. In particular, the trajectory equation

$$\frac{dx_{p,i}}{dt} = u_{p,i} \tag{4.4}$$

is integrated to obtain the position of the particle from its velocity, the latter computed from the equation of motion

$$\frac{4}{3}\pi\rho_p a^3 \frac{du_{p,i}}{dt} = 6\pi\rho\nu a(u_i - u_{p,i}). \tag{4.5}$$

The Navier-Stokes equations (4.1)-(4.2) are solved with a finite-difference discretization of second order central in space and fourth-order Runge-Kutta in time (Pouransari *et al.* 2015). The input parameters of the simulations are $L = 2\pi$, $\nu = 0.05$, $k_\infty = 552$ and $G = 100$, all quantities being expressed in arbitrary yet consistent units. The resulting Taylor-Reynolds number of the turbulence is $\mathrm{Re}_\lambda = 85$. The calculations are conducted on a staggered, uniform cartesian grid of $N^3 = 256^3$ points, which translates into a resolution $\kappa_{max}\ell_k = 1.56$, where κ_{max} is the largest wavenumber resolved by the grid. The grid allows $S = 8$ levels of wavelet resolution, with $\ell_1 = 4\ell_k$ corresponding to the first level $s = 1$. The Kolmogorov-based Stokes number (2.10) used in the computations ranges from 0.1 to 40. The simulations therefore involve cases of small and large particle inertia relative to the small scales of the turbulence. These values of St_k translate into large-scale Stokes numbers $\mathrm{St}_\ell = t_a/t_\ell$ in the range $0.005 - 2$.

After the turbulence has reached a statistically steady state, $N_p = 10^7$ particles are randomly seeded in the computational domain under kinematic equilibrium with the carrier phase. The particle concentration is computed by projecting the Lagrangian particles on an Eulerian grid with 128^3 grid points, which warranted that each cell contained, on average, at least 5 particles. The corresponding number of wavelet resolution levels for concentration is $S = 7$. Data collection starts after a time sufficiently long compared to the characteristic particle acceleration time has passed, and it lasts for a period $16t_\ell$ during which 20 snapshots are recorded for time-averaging the statistics computed using the wavelet formulation described in Section 3.

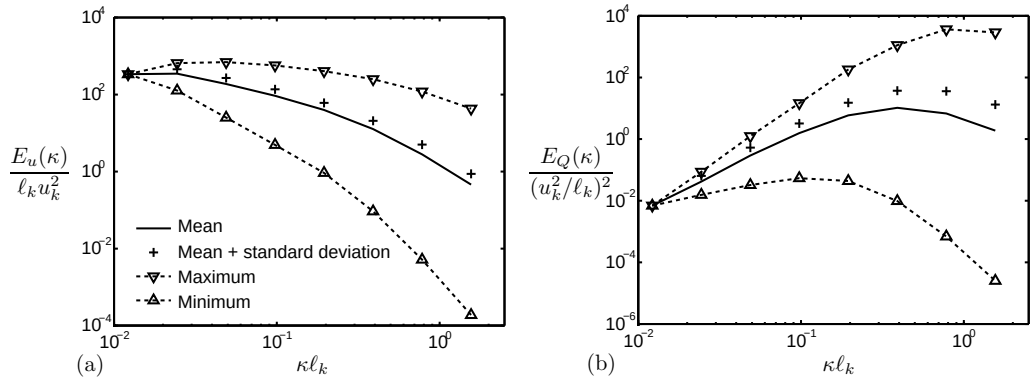

FIGURE 3. Wavelet spectra of (a) kinetic energy and (b) Q-fluctuation energy. The symbols denote the wavelet resolution levels $s = 1, 2, \ldots 8$, with $\ell_s/2\ell_k = 2^s$.

5. Wavelet-based particle-laden turbulence statistics

Spectral energetics of velocity and Q fluctuations are provided in Figure 3. The data portray spatially-averaged wavelet spectra given by Eq. (3.7), which are reminiscent of Fourier spectra. Also included are the standard deviation and spectra extrema, as computed from Eqs. (3.9) and (3.11), respectively, which correspond to spatial variations of the spectral dynamics. These variations, which highlight the scale-dependent spatial intermittency of turbulence and cannot be captured by regular Fourier transforms, render a gap of six orders of magnitude in energy extrema at Kolmogorov scales.

5.1. *Turbulence spectra*

The spatial localization properties of the wavelet transform provide information about spectral dynamics of the turbulence surrounding the particles. For instance, Figure 4 shows the ratio of concentration-weighted spectra $\widetilde{E}(\kappa)$ to unweighted spectra $E(\kappa)$ for kinetic energy and Q, which are plotted as functions of the wavenumber. As described in Section 3, the concentration weighting takes into account the amount of particles at the scale and spatial location where the spectra are computed. At small wavenumbers, the spectra ratio $\widetilde{E}(\kappa)/E(\kappa)$ approaches unity, indicating that no discernible preferential concentration takes place at these scales. Similarly, the spectra ratio theoretically asymptotes to unity for infinitely large and vanishingly small Stokes numbers, for which the particles are either tracers or follow ballistic trajectories, respectively, thereby sampling all turbulent structures without bias introduced by preferential-concentration effects. However, at intermediate Stokes numbers, the spectra ratio decays to values smaller than unity. This phenomenon is a signature of preferential concentration, as described schematically in Figure 2, and evolves non-monotonically with the Stokes number as well. Specifically, the decay of the spectra ratio indicates that the particle clouds low-pass filter the mean ambient turbulence, in that they preferentially sample relatively calmer regions of the flow (approx. 15% and 40% calmer in velocity and Q fluctuations, respectively) subjected to decreasingly less fluctuations than the mean level as the wavenumber increases.

The tendency of particle clouds to move into flow regions undergoing low levels of fluctuations is a scale-dependent phenomenon. This is observed in Figure 5, which depicts the spectra ratio as a function of the Stokes number (2.10) for different wavenumbers. In particular, the results show that the decrement of turbulence fluctuations in the surroundings of the particle clouds is most pronounced for the small scales, where the inter-

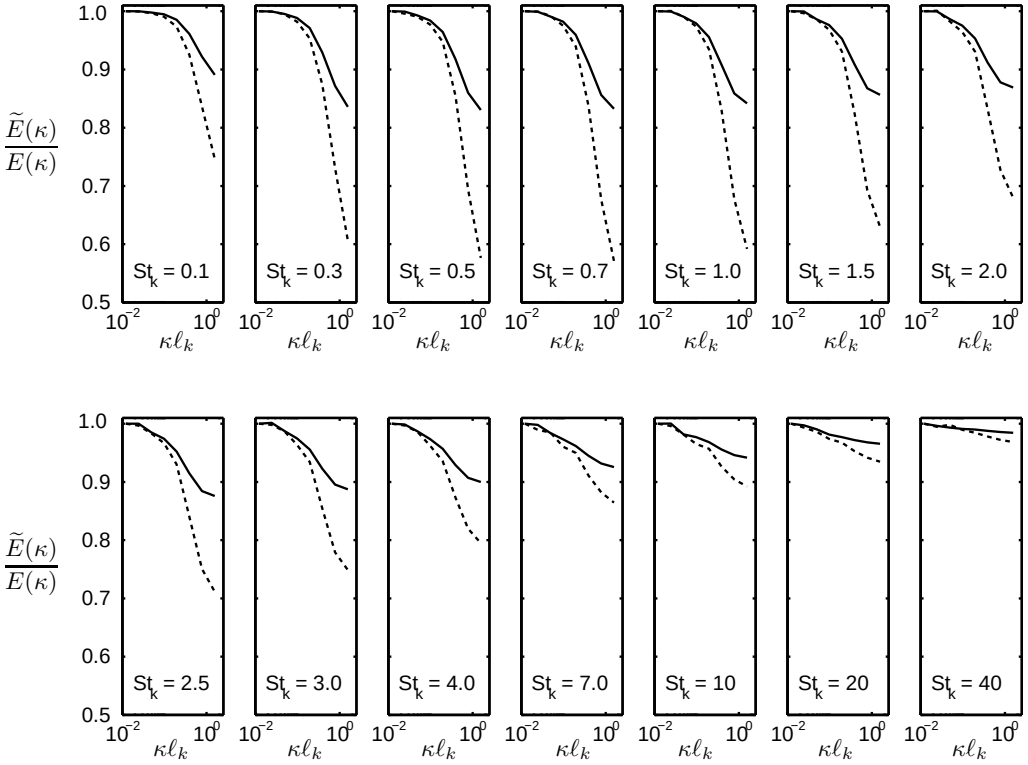

FIGURE 4. Ratio of concentration-weighted spectra to unweighted spectra versus wavenumber for velocity (solid line) and second invariant of the velocity-gradient tensor (dotted line).

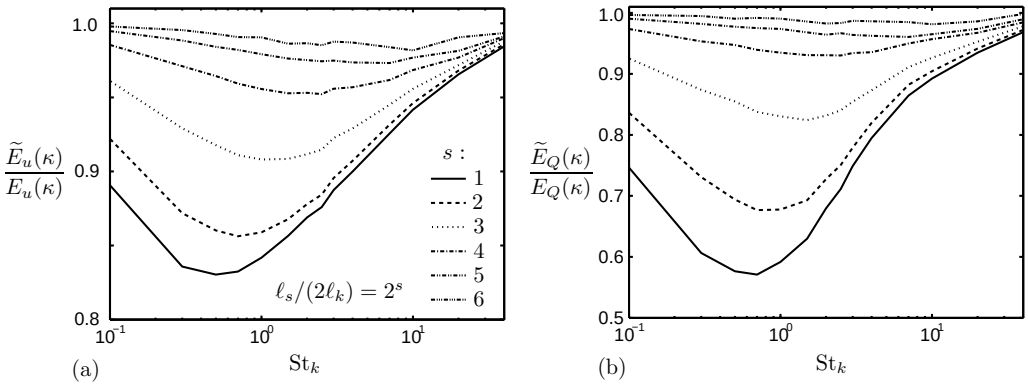

FIGURE 5. Scale repartition of the ratio of concentration-weighted spectra to unweighted spectra versus Stokes number for (a) velocity and (b) second invariant of the velocity-gradient tensor.

mittency is the largest. However, per scale, the peak of fluctuation downsampling occurs at different Stokes numbers, which is a consequence of the fact that particle-turbulence relative motion is most amplified with respect to eddies whose Stokes number is of order unity based on their turnover time (Urzay *et al.* 2014). These considerations are further

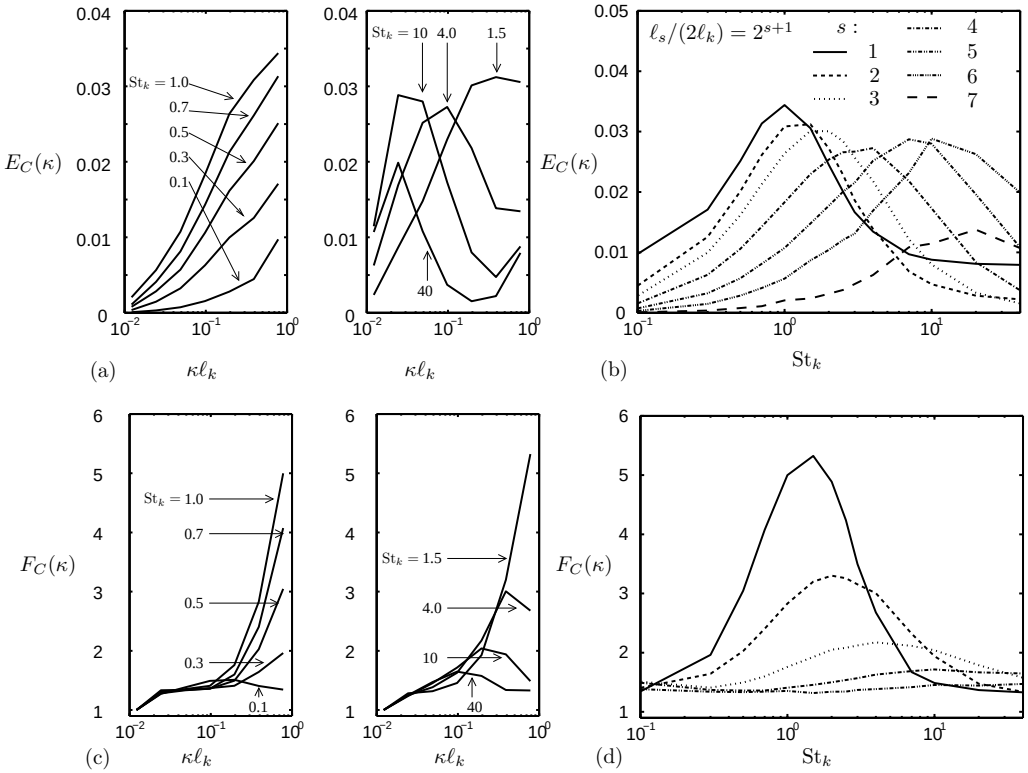

FIGURE 6. Mean wavelet spectrum of particle concentration field (upper panels) and spectral flatness factor (bottom panels) versus wavenumber for different Stokes number (a,c) and versus Stokes number for different wavenumbers (b,d).

explained in Section 5.3, where it is shown that the curves in Figure 5 collapse along the horizontal axis if an appropriate spatial scaling is used for the Stokes number.

5.2. *Concentration spectra*

In homogeneous-isotropic turbulence, preferential concentration arises when the characteristic particle acceleration time becomes comparable to the Kolmogorov turnover time, as observed in the DNS snapshot for $\mathrm{St}_k = 1$ shown in Figure 2. A spectral representation of this phenomenon is provided in Figure 6(a,b) in terms of the mean concentration spectrum E_C, which quantifies the energy associated with the spatial fluctuations of C caused by preferential concentration. In particular, it is observed that the characteristic scale associated with the peak in E_C is a Stokes-number-dependent one that moves from large to small wavenumbers as the Stokes number decreases. Similarly, the energy of the concentration fluctuations decreases rapidly as the Stokes number departs from order-unity values, thereby implying an increasingly uniform spatial distribution of particles and a diminishing importance of preferential concentration. These considerations are in agreement with previous analyses based on Fourier transforms (Jin *et al.* 2010).

While Figure 6(a,b) shows spatially-averaged dynamics, the results displayed in Figure 6(c,d) provide wavelet-enabled information of the spatial variability of E_C in terms of the flatness factor defined in Eq. (3.10). Specifically, the analysis shows that the high-wavenumber peaks of E_C associated with preferential concentration have larger flatness

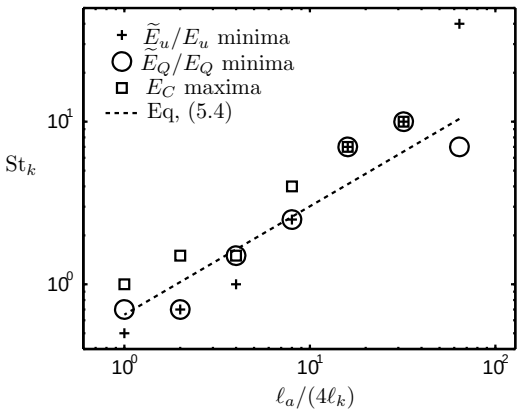

FIGURE 7. Eddy scale for maximum particle response versus the Stokes number associated with the spectra-ratio minima and the concentration-spectra maxima observed, respectively, in Figures 5 and 6(b).

factors, indicating an increased intermittency in the spatial distribution of particles as the Stokes number approaches order-unity values. This is in contrast to the smaller flatness factors associated with the peaks in E_C at large or small Stokes numbers, which suggest an increasingly organized particle distribution in absence of preferential-concentration effects. In conclusion, although peaks are observed in E_C for Stokes numbers away from order-unity values, they are much less spatially intermittent than the peaks in E_C observed for preferentially concentrated regimes at order-unity values of St_k.

5.3. *Eddy scale for maximum particle response*

The wavelet-based spectral results in Figures 4-5 provide direct spectral information of the turbulence in the surroundings of the particle clouds in wavenumber space. This is in contrast to analyses performed in the Lagrangian frame that describe dynamics of the flow velocity seen by the particles by Fourier-transforming the velocity signals into frequency space. Wavenumbers are representative of the spatial scales of turbulence in the vicinity of the preferentially concentrated particle clouds. The fluctuation frequencies recorded in the Lagrangian frame attached to the inertial particles are not straightforwardly related to the spatial scales of the underlying turbulence. An approximate relation between spatial and temporal dynamics, useful for tracers, can be foreseen using Kolmogorov's universal scaling,

$$t_s \sim (\ell_s^2/\epsilon)^{1/3}, \tag{5.1}$$

where ℓ_s is the eddy size and t_s is the corresponding turnover time. Using Eq. (5.1), the Stokes number (2.10) can be written as

$$\mathrm{St}_k = \mathrm{St}_s(\ell_s/\ell_k)^{2/3}, \tag{5.2}$$

where St_s is a scale-dependent Stokes number given by

$$\mathrm{St}_s = t_a/t_s. \tag{5.3}$$

As described in Urzay *et al.* (2014), the relative motion between the particle and the ambient turbulence becomes most amplified for eddies whose Stokes number St_s is of

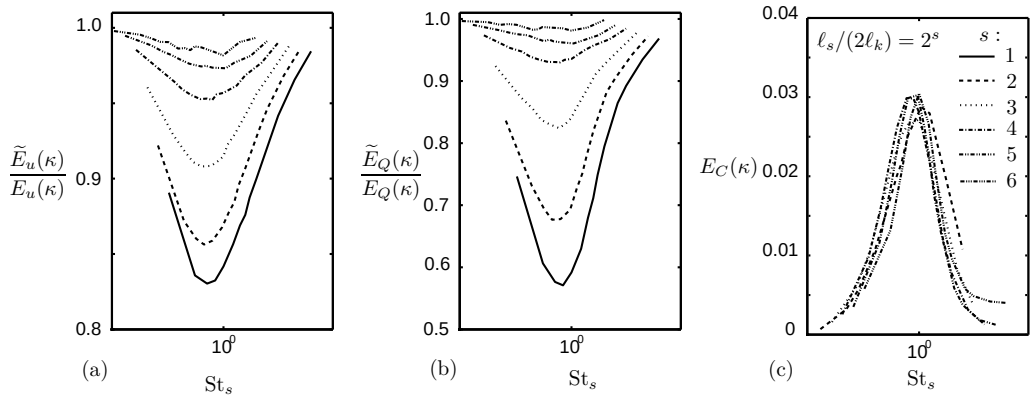

FIGURE 8. (a,b) Figure 5 and (c) Figure 6(b) replotted using the scale-dependent Stokes number St_s instead of St_k in the horizontal axis.

order unity, or equivalently, for eddies whose characteristic size is of order

$$\frac{\ell_a}{\ell_k} \sim \mathrm{St}_k^{3/2}, \tag{5.4}$$

where use of Eq. (5.2) has been made. It is noteworthy that the power relation (5.4) is a good approximation to describe the Stokes number associated with the spectra-ratio minima and the concentration-spectra maxima observed, respectively, in Figures 5 and 6(b), as shown in Figure 7. These considerations suggest that the dynamics portrayed in Figures 5 and 6(b) are manifestations of particle maximum response to eddies of length scale ℓ_a given by Eq. (5.4). This can also be understood by replotting Figures 5 and 6(b) in terms of St_s rather than St_k, which leads to collapse of the curves with respect to the horizontal axis, as shown in Figure 8, with all maxima and minima being aligned with the relevant Stokes number $\mathrm{St}_s \sim 1$ for which the slip velocity is maximum.

6. Concluding remarks

In contrast to regular Fourier analyses, the wavelet transform enables extraction of spatially-localized spectral dynamics. In this study, wavelets are used to analyze the turbulent flow in the surroundings of preferentially concentrated particle clouds in terms of spectral densities of fluctuations of velocity and second invariant velocity-gradient tensor (denoted as Q). Additionally, the spatial variabilities of the concentration spectra are addressed using wavelet-enabled statistical moments. The analysis is focused on DNS of one-way coupled, incompressible homogeneous-isotropic turbulence. In this flow, preferential concentration occurs in regimes where particles interact with the small scales of turbulence, in such a way that the associated Kolmogorov-scale-based Stokes number is of order unity.

The results of this investigation suggest that, in preferentially concentrated regimes, the particles are found in flow regions undergoing fluctuation levels smaller than the average. Such selective sampling of the small turbulence scales is enabled by their high intermittency, which allows the particles to concentrate preferentially in small scales where the strain rate is maximum while avoiding high-wavenumber flow structures of high vorticity. The preferentially concentrated clouds are clearly distinguishable by a peak in the concentration spectra, with the associated characteristic scales being of the

same order as the Kolmogorov length. In turn, as the regime of preferential concentration is approached, the high-wavenumber range of the concentration spectra, where the peak is observed, becomes increasingly intermittent in space.

It should be stressed here that in the present study preferential concentration is associated with interaction of particles with small scales of turbulence. This is an appropriate description for homogeneous-isotropic turbulence, where Kolmogorov eddies are frequently observed everywhere in the flow. In different types of flow configurations, such as particle-laden turbulent jets or mixing layers, the coherency of the large-scale eddies produces preferential concentration in regimes where the characteristic particle acceleration time becomes of the same order as the integral time instead, with particles accumulating along saddle zones perpendicular to the braids in between the large-scale vortices (Lazaro & Lasheras 1989; Longmire & Eaton 1992). In those flows, the description given here may require revision, although in principle the lack of triple periodicity does not represent there an obstacle for wavelet-based spectral analyses.

Acknowledgments

This investigation was funded by the Advanced Simulation and Computing (ASC) program of the US Department of Energy's National Nuclear Security Administration via the PSAAP-II Center at Stanford.

REFERENCES

Balachandar. S. & Eaton, J. K. 2010 Turbulent dispersed multiphase flow. *Annu. Rev. Fluid Mech.* **42**, 111–133.

Bassenne, M., Urzay, J., Park, G. I. & Moin, P. 2015 Constant-energetics physical-space forcing methods for improved convergence to homogeneous-isotropic turbulence with application to particle-laden flows. Submitted to *Phys. Fluids.*

Farge, M. & Rabreau, G. 1988 Transformee en ondelettes pour detecter et analyser les structures coherentes dans les acoulements turbulents bidimensionnels. *Compt. Rend. Acad. Sci.* **307**, 1479-1486.

Fernández De La Mora, J. & Riesco-Chueca P. 1988 Aerodynamic focusing of particles in a carrier gas. *J. Fluid Mech.* **195**, 1–21.

Ferrante, A. & Elghobashi, S. 2003 On the physical mechanisms of two-way coupling in particle-laden isotropic turbulence. *Phys. Fluids* **15**, 315-329.

Jin, G., He, G.W. & Wang L. P. 2010 Large-eddy simulation of turbulent collision of heavy particles in isotropic turbulence. *Phys. Fluids* **22**, 055106.

Lazaro, B. J. & Lasheras, J. C. 1989 Particle dispersion in a turbulent plane shear layer. *Phys. Fluids* **1**, 1035-1044.

Longmire, E. K. & Eaton, J. K. 1992 Structure of a particle-laden round jet. *J. Fluid Mech.* **236**, 217-257.

Mallat, S. G. 1989 A theory for multiresolution signal decomposition: the wavelet representation. *Pattern Analysis and Machine Intelligence, IEEE Transactions.* **11**, 674-693.

Maxey, M. R. 1987 The gravitational settling of aerosol particles in homogeneous turbulence and random flow fields. *J. Fluid Mech.* **174**, 441-465.

Meneveau, C. 1991 Analysis of turbulence in the orthonormal wavelet representation. *J. Fluid Mech.* **232**, 469-520.

Passot, T & Pouquet, A. 1987 Numerical simulation of compressible homogeneous flows in the turbulent regime. *J. Fluid Mech.* **181**, 441-466.

Pouransari, H., Mortazavi, M. & Mani, A. 2015 Parallel variable-density particle-laden turbulence simulation. *Annual Research Briefs*, Center for Turbulence Research, Stanford University, pp. 43-54.

Robinson, A. 1956 On the motion of small particles in a potential field of flow. *Comm. Pure Appl. Math.* **9**, 69–84.

Sánchez, A. L., Urzay, J. & Liñán, A. 2014 The role of separation of scales in the description of spray combustion. *Proc. Combust. Inst.* **35**, 1549–1577.

Schneider, K. & Vasilyev, O.V. 2010 Wavelet methods in computational fluid dynamics. *Annu. Rev. Fluid Mech.* **42**, 473-503.

Squires, K.D. & Eaton, J.K. 1991 Preferential concentration of particles by turbulence. *Phys. Fluids* **3**, 1169-1178.

Urzay J., Bassenne M., Park G.I. & Moin P. 2014 Characteristic regimes of subgrid-scale coupling in LES of particle-laden turbulent flows. *Annual Research Briefs*, Center for Turbulence Research, Stanford University, pp. 3-13.

Wang, L.P. & Maxey, M.R. 1987 Settling velocity and concentration distribution of heavy particles in homogeneous isotropic turbulence. *J. Fluid Mech.* **256**, 27-68.